Grain Segmentation of 3D Superalloy Images Using Multichannel EWCVT under Human Annotation Constraints

Yu Cao[1], Lili Ju[2], and Song Wang[1]

[1] Department of Computer Science & Engineering,
[2] Department of Mathematics
University of South Carolina, Columbia, SC 29208, USA
{cao,songwang}@cec.sc.edu, ju@math.sc.edu

Abstract. Grain segmentation on 3D superalloy images provides superalloy's micro-structures, based on which many physical and mechanical properties can be evaluated. This is a challenging problem in senses of (1) the number of grains in a superalloy sample could be thousands or even more; (2) the intensity within a grain may not be homogeneous; and (3) superalloy images usually contains carbides and noises. Recently, the *Multichannel Edge-Weighted Centroid Voronoi Tessellation* (MCEWCVT) algorithm [1] was developed for grain segmentation and showed better performance than many widely used image segmentation algorithms. However, as a general-purpose clustering algorithm, MCEWCVT does not consider possible prior knowledge from material scientists in the process of grain segmentation. In this paper, we address this issue by defining an energy minimization problem which subject to certain constraints. Then we develop a *Constrained Multichannel Edge-Weighted Centroid Voronoi Tessellation* (CMEWCVT) algorithm to effectively solve this constrained minimization problem. In particular, manually annotated segmentation on a very small set of 2D slices are taken as constraints and incorporated into the whole clustering process. Experimental results demonstrate that the proposed CMEWCVT algorithm significantly improve the previous grain-segmentation performance.

1 Introduction

For different industrial applications, engineers need to choose proper kinds of superalloys with desired mechanical or physical properties, such as lightness, hardness, stiffness, electrical conductivity and fluid permeability [2]. Such properties are related to the micro-structures of the superalloy material which is usually made up of a set of grains [3]. Thus, in the repeated development or researches on superalloy materials, the major task is to identify the superalloy micro-structures so that their mechanical and physical properties can be evaluated. Currently, material scientists mainly conduct manual annotations/segmentations on 2D superalloy image slices and then combine the 2D results to reconstruct the 3D grains.

A. Fitzgibbon et al. (Eds.): ECCV 2012, Part III, LNCS 7574, pp. 244–257, 2012.

Given the large number of grains in a superalloy sample and the large number of slices in its high-resolution 3D microscopic images, this manual-segmentation process is very tedious, time consuming and prone to error. Manual segmentation becomes even more difficult when the microscopic superalloy images are multi-channel images, where different channels reflect different parameter settings of the electronic microscope. For example, Figure 1 shows four channels of a single 2D slice, from which we can see that adjacent grains may be distinguishable by their intensity in certain channels but not in other channels. As a result, we may need to manually segment the image in each channel and then combine the segmentation results from different channels.

In principle, many existing segmentation methods may be useful to relieve material scientists from the manual segmentation. 2D segmentation methods, such as mean shift [4], watershed [5], statistical region merging [6], normalized cuts [7], graph cuts [8], level set [9] and watershed cuts [10, 11], can be applied to segment 2D slices. Especially, in [12], a region merging segmentation method called "the stabilized inverse diffusion equation" and a stochastic segmentation method called "the expectation-maximization/maximization of the posterior marginals (EM/MPM) algorithm" are combined for 2D Ni-based superalloy image segmentation. However, all the above 2D segmentation methods still cannot effectively and accurately correspond the segments across adjacent slices to achieve the desired 3D grain segmentation.

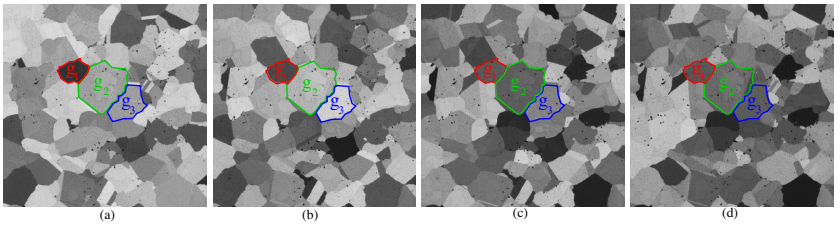

Fig. 1. Microscopic images of a slice of the superalloy sample taken by using 4 different microscope settings. Small black points in the images are carbides. (a) 4000_Series. (b) 5000_Series. (c) 6000_Series. (d) 7000_Series.

3D image segmentation methods [13–16] can segment a volume image to achieve 3D grains directly. Recently, Cao et al. developed a *Multichannel Edge-Weighted Centroid Voronoi Tessellation* (MCEWCVT) algorithm for 3D multichannel superalloy grain segmentation, which outperforms many existing segmentation algorithms [1]. In MCEWCVT, the voxels in a 3D volume image are clustered into a set of groups which then form a segmentation on the 3D image space. The clustering is achieved by an unconstrained minimization of an energy function which combines a multichannel clustering energy term called "similarity" and an edge energy term called "regularity". The "similarity" term measures the distances from each voxel's multichannel intensity to the center of a cluster (in multichannel intensity space) to which the voxel is clustered. The

"regularity" term measures the amount of segmentation edges in image space. Thus, when the MCEWCVT energy function is minimized, the voxels sharing similar multichannel intensities are grouped into the same cluster while the small over-segmentations are suppressed.

However, the MCEWCVT algorithm has two limitations: 1) the number of clusters is empirically chosen and the initial clusters are randomly generated; 2) no existing prior knowledge from material scientists is incorporated into the segmentation process. In practice, the prior knowledge could include the geometry on the grains' layout, the grains' phase identifications, and the grains' intensity similarity in different channels, etc. Material scientists have been exploring such kinds of prior knowledge for decades, and using them when they manually annotate the segmentations of 3D superalloy grains. In this paper, we incorporate such prior knowledge into the MCEWCVT model to further improve the grain segmentation performance. Specifically, we first construct a constrained minimization problem by enforcing a set of human annotated constraints (coming from a few manually segmented 2D slices) into the original MCEWCVT model. Then we develop a *constrained multichannel edge-weighted centroid Voronoi tessellation* (CMEWCVT) algorithm to solve the constrained minimization problem. In this algorithm, we also use the human annotated constraints to help determine the proper cluster numbers and the initial cluster centers.

The remainder of this paper is organized as follows. In Section 2, we briefly review the MCEWCVT model. The new constrained energy minimization problem is proposed in Section 3, and then we develop an effective CMEWCVT algorithm for solving the proposed problem in Section 4. We report the experimental and comparison results in Section 5. Section 6 concludes the paper.

2 The Multichannel Edge-Weighted Centroidal Voronoi Tessellation Model

In [1], segmentation of a multichannel superalloy volumetric image is mathematically formalized as an unconstrained minimization problem in which the energy (cost) function consists of a multichannel clustering energy term called "similarity" and an edge energy term called "regularity". Such a minimization problem can be effectively solved by an iterative MCEWCVT algorithm which guarantees decreasing of the energy in each iteration. In this section, we briefly review this algorithm for superalloy segmentation.

2.1 Multichannel Edge-Weighted Clustering Energy

Let N denote the number of image channels of the superalloy volume, i.e., we have N images, $u^1, u^2, \ldots, u^N$, of the same superalloy sample taken under N different microscope parameter settings. The set of intensity values of the 3D superalloy images $\mathbb{U}$ and the *generators* $\mathcal{W}$ can be written in the vector form as

$$\mathbb{U} = \{\boldsymbol{u}(i,j,k) = (u^1, u^2, \cdots, u^N)^T \in \mathbb{R}^N\}_{(i,j,k)\in D}$$

and

$$\mathcal{W} = \{\boldsymbol{w}_l = (w_l^1, w_l^2, \cdots, w_l^N)^T \in \mathbb{R}^N\}_{l=1}^L,$$

respectively. Note here L denotes the number of generators and $D = \{(i,j,k)|i = 1,\ldots,I, j = 1,\ldots,J, k = 1,\ldots,K\}$ is an index set for a superalloy volume domain. The *multichannel clustering energy* can be defined as

$$E_C(\mathcal{W};\mathcal{D}) = \sum_{l=1}^{L} \sum_{(i,j,k)\in D_l} \rho(i,j,k)\|\boldsymbol{u}(i,j,k) - \boldsymbol{w}_l\|_\infty^2 \tag{1}$$

where $\mathcal{D} = \{D_l\}_{l=1}^L$ is a tessellation of the image domain D and ρ is a predefined density function over D.

For each voxel $(i,j,k) \in D$, we denote $\mathbb{N}_\omega(i,j,k)$ a local neighborhood for it, which could be a $2\omega \times 2\omega \times 2\omega$ cube centered at (i,j,k) or a sphere centered at (i,j,k) with radius ω. Further if we define a local characteristic function $\chi_{(i,j,k)} : \mathbb{N}_\omega(i,j,k) \to \{0,1\}$ as

$$\chi_{(i,j,k)}(i',j',k') = \begin{cases} 1 & \text{if } \pi_u(i',j',k') \neq \pi_u(i,j,k) \ , \\ 0 & \text{otherwise,} \end{cases}$$

where $\pi_u(i,j,k) : D \to \{1,\ldots,L\}$ tells which cluster $\boldsymbol{u}(i,j,k)$ belongs to, then similar to [17], an edge energy can be defined as

$$E_L(\mathcal{D}) = \sum_{(i,j,k)\in D} \sum_{(i',j',k')\in\mathbb{N}_\omega(i,j,k)} \chi_{(i,j,k)}(i',j',k'). \tag{2}$$

When the density function ρ is defined as $\rho = 1 + |\nabla \boldsymbol{u}|$, the total energy function, i,e., the *multichannel edge-weighted clustering energy*, is defined as:

$$\begin{aligned} E(\mathcal{W};\mathcal{D}) &= E_C(\mathcal{W};\mathcal{D}) + \lambda E_L(\mathcal{D}) \\ &= \sum_{l=1}^{L} \sum_{(i,j,k)\in D_l} (1 + |\nabla \boldsymbol{u}(i,j,k)|)\|\boldsymbol{u}(i,j,k) - \boldsymbol{w}_l\|_\infty^2 \\ &\quad + \lambda \sum_{(i,j,k)\in D} \sum_{(i',j',k')\in\mathbb{N}_\omega(i,j,k)} \chi_{(i,j,k)}(i',j',k'), \end{aligned} \tag{3}$$

where λ is a weighting parameter to control the balance between E_C and E_L. Thus, the desired 3D superalloy segmentation result are

$$(\tilde{\mathcal{W}};\tilde{\mathcal{D}}) = \arg\min_{(\mathcal{W};\mathcal{D})} E(\mathcal{W};\mathcal{D}). \tag{4}$$

2.2 Energy Minimizer and MCEWCVT

As proved in [1], moving a voxel (i,j,k) to the cluster of a generator to which it has the shortest *multichannel edge-weighted distance* will decrease the total

clustering energy $E(\mathcal{W};\mathcal{D})$ at the most, where the multichannel edge-weighted distance can be defined as

$$\begin{aligned} dist((i,j,k),\boldsymbol{w}_l) &= \sqrt{\rho(i,j,k)\|\boldsymbol{u}(i,j,k)-\boldsymbol{w}_l\|_\infty^2 + 2\lambda\tilde{n}_l(i,j,k)} \\ &= \sqrt{(1+|\nabla\boldsymbol{u}(i,j,k)|)\|\boldsymbol{u}(i,j,k)-\boldsymbol{w}_l\|_\infty^2 + 2\lambda\tilde{n}_l(i,j,k)} \end{aligned} \tag{5}$$

with $\tilde{n}_l(i,j,k)$ denotes the number of voxels in $\mathbb{N}_w(i,j,k)\backslash(D_l \bigcup (i,j,k))$.

Given a set of generators $\mathcal{W} = \{\boldsymbol{w}_l\}_{l=1}^L$, the *multichannel edge-weighted Voronoi tessellation* (MCEWVT) $\tilde{\mathcal{D}} = \{\tilde{D}_l\}_{l=1}^L$ associated with the generators $\mathcal{W}$ in the physical volume space D can be defined as

$$\tilde{D}_l = \{(i,j,k) \in D \mid dist((i,j,k),\boldsymbol{w}_l) \le dist((i,j,k),\boldsymbol{w}_m), m = 1,\ldots,L\}. \tag{6}$$

When $\mathcal{W}$ is fixed, the MCEWVT $\tilde{\mathcal{D}}$ associated with $\mathcal{W}$ corresponds to the minimizer of the multichannel edge-weighted energy $E(\mathcal{W};\mathcal{D})$, i.e., $\tilde{\mathcal{D}} = \arg\min_{\mathcal{D}} E(\mathcal{W};\mathcal{D})$. On the other hand, given a set of partition $\tilde{\mathcal{D}} = \{\tilde{D}_l\}_{l=1}^L$ of D, their corresponding centroids $\mathcal{W} = \{\boldsymbol{w}_l^*\}_l^L$ are defined to be

$$\boldsymbol{w}_l^* = \arg\min_{\boldsymbol{w}} \sum_{(i,j,k)\in\tilde{D}_l} \rho(i,j,k)||\boldsymbol{u}(i,j,k)-\boldsymbol{w}||_\infty^2, \quad l = 1,\cdots,L. \tag{7}$$

It was shown in [1] that $(\mathcal{W};\tilde{\mathcal{D}})$ is a minimizer of $E(\mathcal{W};\tilde{\mathcal{D}})$ only if $(\mathcal{W};\tilde{\mathcal{D}})$ forms a *multichannel edge-weighted centroidal Voronoi tessellation* (MCEWCVT), i.e., $\mathcal{W}$ are simultaneously the corresponding centroids of the associated multichannel edge-weighted Voronoi regions $\{\tilde{D}_l\}_{l=1}^L$.

3 Constrained 3D Superalloy Grain Segmentation

To improve 3D multichannel superalloy grain image segmentation, we may use human annotated segmentation results on a small set of pre-selected superalloy slices as the prior knowledge, i.e., constraints from the problem domain.

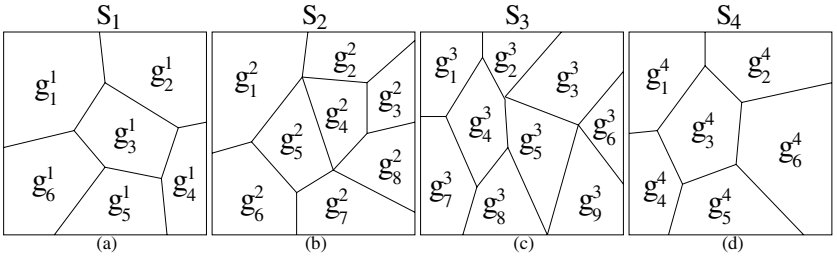

Fig. 2. Illustrations of the segmentation constraints on some pre-selection image slices

As illustrated in Fig. 2, 2D human annotated segmentations $\mathcal{S} = \{\mathcal{S}_m\}_{m=1}^M$ on M (pre-selected) constraint superalloy image slices (the segmentations are

annotated by considering all the channels) can be written as $\mathcal{S}_m = \cup_{n=1}^{N_m} g_n^m$ where g_n^m denotes the n-th 2D grain region on the m-th constraint superalloy image slice, N_m is the number of grains on m-th constraint superalloy image according to the annotated segmentation. It satisfies

$$g_n^m \cap g_{n'}^{m'} = \emptyset, \quad \text{if } n \neq n'. \tag{8}$$

Thus the constraints over the tessellation (or say grouped clusters) $\mathcal{D}$ can be defined mathematically as:

$$\begin{aligned} &\mathcal{C}_1(\mathcal{D}) = \{\Psi(p) = \Psi(q), \ \ \forall\, p, q \in g_n^m\} \\ &\mathcal{C}_2(\mathcal{D}) = \{\Psi(p) \neq \Psi(q), \ \ \forall\, p \in g_n^m, q \in g_{n'}^m, g_n^m \text{ and } g_{n'}^m \text{ are neighbor grains}\} \end{aligned} \tag{9}$$

where $\Psi(\cdot)$ denotes the generic form of the clustering function which provides a cluster label for a given voxel. Thus we can define the 3D multichannels superalloy image segmentation problem under such human annotation constraints to be a constrained energy minimization problem in the form of

$$(\tilde{\mathcal{W}}; \tilde{\mathcal{D}}) = \arg \min_{(\mathcal{W};\mathcal{D})} E(\mathcal{W}; \mathcal{D}) \quad \text{subject to} \quad \mathcal{C} = \{\mathcal{C}_1(\mathcal{D}) \,\&\, \mathcal{C}_2(\mathcal{D})\}. \tag{10}$$

We would like to point out that the above defined constraints namely only take effect on the voxels within the same constraint 2D superalloy slice, but it is expected that those constraints will propagate their effects to other non-constraint slices during the solution process to give improved grain segmentations.

4 Constrained Multichannel Edge-Weighted Centroid Voronoi Tessellation Algorithm

In the following, we will develop a *constrained multichannel edge-weighted centroid Voronoi tessellation* (CMEWCVT) algorithm to solve the above constrained minimization problem. In the algorithm we first enforce the initial clusters to satisfy constraint $\mathcal{C}$. And then the constraint is imposed on the whole energy minimization process.

Denote the average multichannel intensities of grains $g_n^m \in \mathcal{S}$ to be

$$\mathbb{U}^c = \{\boldsymbol{u}_1^1, \boldsymbol{u}_2^1, \cdots, \boldsymbol{u}_{N_1}^1, \boldsymbol{u}_1^2, \boldsymbol{u}_2^2, \cdots, \boldsymbol{u}_{N_2}^2, \cdots, \boldsymbol{u}_1^M, \cdots, \boldsymbol{u}_{N_M}^M\}. \tag{11}$$

4.1 Determine an Initial Configuration Satisfying Constraints

We first run the K-means on $\mathbb{U}^c$ with a small cluster number using a random initialization. Let G be the neighbor graph of the grains in $\mathcal{S}$. If there exist adjacent grains on the same constraint image slices g_n^m and $g_{n'}^m$ whose average intensities $\boldsymbol{u}_n^m$ and $\boldsymbol{u}_{n'}^m$ are clustered into a same cluster, we add a new cluster whose generator is either $\boldsymbol{u}_n^m$ or $\boldsymbol{u}_{n'}^m$. Using the new set of generators to run the K-means on $\mathbb{U}^c$ again. We repeat this process until we obtain a set of clusters which can group $\mathbb{U}^c$ with no adjacent grains on the same constraint image slice belonging to the same cluster. We then define the centers of the these clusters as the initial generators for the CMEWCVT. See Algorithm 1 for the description of the whole procedure.

Algorithm 1. ($\mathcal{W}^c$=$\{\boldsymbol{w}_l^c\}_{l=1}^L$, $\tilde{\mathcal{D}}^{\mathcal{S}}$=$\{\tilde{D}_l^S\}_{l=1}^L, L$) = ConstrainedGenerators($\mathbb{U}^c$, G, $\mathcal{S}$, L_0)

1: INPUT: Human annotated segmentation on certain superalloy image slices $\mathcal{S}$. The average intensities $\mathbb{U}^c$ of grain regions in $\mathcal{S}$. Grain's neighboring matrix G. Initial cluster number guess L_0.
2: START:
3: $L = L_0$ and randomly initialized L cluster generators $\mathcal{W} = \{\boldsymbol{w}_l\}_{l=1}^L$.
4: Run the classic K-means on $\mathbb{U}^c$ with $\mathcal{W}$ to obtain a clustering of $\mathbb{U}^c$.
5: $\tilde{\mathcal{D}}^{\mathcal{S}} \leftarrow \{\tilde{D}_l^s\}_{l=1}^L$: If $\boldsymbol{u}_n^m$ belongs to the cluster with generator $\boldsymbol{w}_l$, then all voxels in g_n^m are in $\tilde{D}_l^s$.
6: **if** Existing g_n^m, $g_{n'}^m$, which belongs to the same cluster, for neighbor grains g_n^m and $g_{n'}^m$ **then**
7: $L = L + 1$
8: $\boldsymbol{w}_L = \boldsymbol{u}_{n'}^m$
9: $\mathcal{W} \leftarrow \{\mathcal{W}, \boldsymbol{w}_L\}$
10: Go to 4.
11: **else**
12: $\mathcal{W}^c = \mathcal{W}$
13: Return ($\mathcal{W}^c$, $\tilde{\mathcal{D}}^{\mathcal{S}}, L$).
14: **end if**

4.2 Constrained Multichannel Edge-Weighted Voronoi Tessellation

In MCEWCVT the clustering energy is minimized by iteratively transferring each voxel from its current cluster to a cluster to which it has the shortest edge-weighted distance defined by Eqn. (5). In the new CMEWCVT model, we need to constrain the transferring of the voxels between clusters. Specifically, we will force the voxels in the constraint grains (in the 2D constraint slices) remains in their original cluster, and for the voxels in the non-constraint image slices, they are allowed to be transfered between clusters.

Given a set of constrained generators $\mathcal{W}^c = \{\boldsymbol{w}_l^c\}_{l=1}^L$ and corresponding constraints $\mathcal{S}$, we define the *constrained multichannel edge-weighted Voronoi tessellation* (CMEWCVT), $\tilde{\mathcal{D}} = \{\tilde{D}_l^c\}_{l=1}^L$ in the physical volume space D as

$$\begin{aligned}\tilde{D}_l^c = \{(i,j,k) \in & D \backslash \mathcal{S} \mid dist((i,j,k), \boldsymbol{w}_l^c) \leq \\ & dist((i,j,k), \boldsymbol{w}_m^c),\ m = 1, \cdots, L\} \ \cup \ \tilde{D}_l^{\mathcal{S}},\end{aligned} \tag{12}$$

where (i,j,k) refers to the voxel on the non-constraint image slices. $\tilde{\mathcal{D}}^{\mathcal{S}}$ is given by Algorithm 1. Thus, we can define the constrained multichannel edge-weighted clustering energy as

$$\begin{aligned}E(\mathcal{W}^c; \mathcal{D}; \mathcal{S}) &= E_C(\mathcal{W}^c; \mathcal{D}; \mathcal{S}) + \lambda E_L(\mathcal{D}) \\ &= \sum_{l=1}^{L} \sum_{(i,j,k) \in \tilde{D}_l^c} (1 + |\nabla \boldsymbol{u}(i,j,k)|) \|\boldsymbol{u}(i,j,k) - \boldsymbol{w}_l^c\|_\infty^2 \\ &\quad + \lambda \sum_{(i,j,k) \in D} \sum_{(i',j',k') \in \mathbb{N}_\omega(i,j,k)} \chi_{(i,j,k)}(i',j',k').\end{aligned} \tag{13}$$

From Eqn. (5), it is also easy to find that when $\mathcal{W}^c$ and $\mathcal{S}$ are fixed, the constrained multichannel edge-weighted Voronoi tessellation $\tilde{\mathcal{D}} = \{\tilde{D}_l^c\}_{l=1}^L$ associated with $\mathcal{W}^c$ and $\mathcal{S}$ corresponds to the minimizer of the constrained multichannel edge-weighted clustering energy $E(\mathcal{W}^c; \mathcal{D}; \mathcal{S})$, i.e.,

$$\tilde{\mathcal{D}} = \arg\min_{\mathcal{D}} E(\mathcal{W}^c; \mathcal{D}; \mathcal{S}).$$

Then we define the *constrained multichannel edge-weighted Voronoi tessellation energy* for a given set of constrained generators $\mathcal{W}^c = \{\boldsymbol{w}_l^c\}_{l=1}^L$ to be

$$E_{CMEWVT}(\mathcal{W}^c, \mathcal{S}) = E(\mathcal{W}^c; \tilde{\mathcal{D}}; \mathcal{S}). \tag{14}$$

Algorithm 2 can be used to effectively construct the constrained multichannel edge-weighed Voronoi tessellation for a given set of constrained generators.

Algorithm 2. $\{\tilde{D}_l^c\}_{l=1}^L$ = CMEWVT($\boldsymbol{u}$,$\{\boldsymbol{w}_l^c\}_{l=1}^L$,$\{D_l^c\}_{l=1}^L$, $\mathcal{S}$)

1: INPUT: A 3D N-channel image determined by $\boldsymbol{u}$, a set of constrained generators $\{\boldsymbol{w}_l^c\}_{l=1}^L$ and an initial constrained partition $\{D_l^c\}_{l=1}^L$ of the physical space D. Human annotated segmentations constraints $\mathcal{S}$.
2: START:
3: **for all** voxels $(i, j, k) \in D$ **do**
4: **if** voxel $(i, j, k) \notin \mathcal{S}$ **then**
5: a) calculate the multichannel edge-weighted distances from the voxel (i, j, k) to all constrained generators $\{\boldsymbol{w}_l^c\}_{l=1}^L$.
6: b) transfer the voxel (i, j, k) from its current cluster to the cluster whose generator has the shortest multichannel edge-weighted distance to it.
7: **end if**
8: **end for**
9: If no voxel in the loop is transferred, return $\{\tilde{D}_l^c\}_{l=1}^L = \{D_l^c\}_{l=1}^L$ and exit; otherwise, go to 3.

4.3 The CMEWCVT Model and Its Construction

In order to define the CMEWCVT model, we need to further determine the centroids of a given set of partition $\tilde{\mathcal{D}} = \{\tilde{D}_l^c\}_{l=1}^L$ of D, i.e., find $\mathcal{W}^c = \{\boldsymbol{w}_l^{c*}\}_{l=1}^L$ such that

$$\boldsymbol{w}_l^{c*} = \arg\min_{\boldsymbol{w}_l^c} \sum_{(i,j,k)\in\tilde{D}_l^c} \rho(i, j, k)\|\boldsymbol{u}(i, j, k) - \boldsymbol{w}_l^c\|_\infty^2 \tag{15}$$

for $l = 1, 2, \cdots, L$. Since we use the $\infty-$norm, it is hard to find an analytical solution for $\boldsymbol{w}_l^c$. Usually, the $\boldsymbol{w}_l^c$ defined through the above minimization process could be solved numerically. For example, the Powell method [18] could be used to effectively calculate $\boldsymbol{w}_l^c$ approximately although there is no derivative information available.

Definition (CMEWCVT). *For a given constrained multichannel edge-weighted Voronoi tessellation* $\left(\{\boldsymbol{w}_l^c\}_{l=1}^L; \{\tilde{D}_l^c\}_{l=1}^L; \mathcal{S}\right)$ *of* D*, we call it a constrained multichannel edge-weighted centroidal Voronoi tessellation (CMEWCVT) of* D *if the generators* $\{\boldsymbol{w}_l^c\}_{l=1}^L$ *are also the corresponding centroids of the associated constrained multichannel edge-weighted Voronoi regions* $\{\tilde{D}_l^c\}_{l=1}^L$*, i.e.,*

$$\boldsymbol{w}_l^c = \boldsymbol{w}_l^{c*}, \quad l = 1, 2, \cdots, L.$$

Based on the CVT principle [19], we know that $(\mathcal{W}^c; \tilde{\mathcal{D}}; \mathcal{S})$ is a minimizer of $E(\mathcal{W}^c; \tilde{\mathcal{D}}; \mathcal{S})$ only if $(\mathcal{W}^c; \tilde{\mathcal{D}}; \mathcal{S})$ forms a CMEWCVT of D. We propose the Algorithm 3 for the construction of the CMEWCVTs. As discussed in [17] for the EWCVT construction algorithms, some improvements of Algorithm 3-CMEWCVT can be obtained by using narrow-banded implementation. We also note that the energy $E_{CMEWVT}(\mathcal{W}^c, \mathcal{S})$ keeps decreasing along the iterations in this algorithm.

Algorithm 3. $(\{\boldsymbol{w}_l^c\}_{l=1}^L, \{\tilde{D}_l^c\}_{l=1}^L)$ = CMEWCVT($\boldsymbol{u}$,L_0,$\mathcal{S}$,G)

1: INPUT: A 3D N-channel images determined by $\boldsymbol{u}$ and initial cluster number guess L_0. Constraints $\mathcal{S}$ and the neighboring graph G of grains in $\mathcal{S}$.
2: START:
3: Construct $\mathbb{U}^c$ using $\mathcal{S}$ and G.
4: $(\{\boldsymbol{w}_l^c\}_{l=1}^L, \{\tilde{D}_l^{\mathcal{S}}\}_{l=1}^L, L)$=ConstrainedGenerators($\mathbb{U}^c, G, \mathcal{S}, L_0$).
5: Construct $\{D_l^c\}_{l=1}^L$ based on $\{\tilde{D}_l^{\mathcal{S}}\}_{l=1}^L$ and Voronoi tessellation on $D\backslash\mathcal{S}$ associated with $\{\boldsymbol{w}_l^c\}_{l=1}^L$ under the Euclidean distance in intensity space.
6: Construct constrained multichannel centroidal Voronoi tessellation regions $\{\tilde{D}_l^c\}_{l=1}^L$=CMEWVT($\boldsymbol{u}$,$\{\boldsymbol{w}_l^c\}_{l=1}^L$,$\{D_l^c\}_{l=1}^L$, $\mathcal{S}$).
7: Calculate cluster centroids $\{\boldsymbol{w}_l^{c*}\}_{l=1}^L$ for $\tilde{D}_l^c, l = 1, \ldots, L$.
8: Take $\{\boldsymbol{w}_l^{c*}\}_{l=1}^L$ as the generators, determine the corresponding constrained multichannel edge-weighted Voronoi clustering $\{\hat{D}_l^c\}_{l=1}^L$ by using Algorithm 2-CMEWVT, i.e., $\{\hat{D}_l^c\}_{l=1}^L$=CMEWVT($\boldsymbol{u}$,$\{\boldsymbol{w}_l^{c*}\}_{l=1}^L$,$\{\tilde{D}_l^c\}_{l=1}^L$, $\mathcal{S}$).
9: If $\{\hat{D}_l^c\}_{l=1}^L$ and $\{\tilde{D}_l^c\}_{l=1}^L$ are the same, set $\{\boldsymbol{w}_l^c\}_{l=1}^L = \{\boldsymbol{w}_l^{c*}\}_{l=1}^L$, return $(\{\boldsymbol{w}_l^c\}_{l=1}^L; \{\tilde{D}_l^c\}_{l=1}^L)$ and exit; otherwise, set $\tilde{D}_l^c = \hat{D}_l^c$ for $l = 1, \ldots, L$ and go to step 7.

5 Experiments and Evaluation

The proposed CMEWCVT algorithm is tested on a Ni-based 3D superalloy image dataset. The dataset consists 4 channels of superalloy slice images taken under different electronic microscope parameters settings. Each slice was photographed as new facets appearing by keeping abrading the up-front facet of the superalloy sample. The size of each image slice is 671×671 and the number of slices in each channel is 170. The resolution within a slice is $0.2\mu m$ and the resolution between slices is $1\mu m$.

The resolution on the 2D superalloy image slice are 5 times higher than that between adjacent image slices. In order to control the smoothness and compactness of the segmentation on 3D superalloy image, we followed [1] by linearly interpolating the 3D superalloy image with 4 more slices between each two original slices. The interpolated superalloy volume image has 846 slices. In order to run the CMEWCVT with more iterations in reasonable time, we downsized the 3D volume image to half of its size along each direction and applied the proposed CMEWCVT algorithm on this downsized superalloy volume image. Finally, we scale the segmentation results back to its original resolution for performance evaluation. There are six parameters/factors that can be controlled in CMEWCVT: L, the number as input for constructing initial clusters' generators; λ, the weighting parameter which balances the clustering energy term and the edge energy term; ω, the neighbor size which defines the local search region $\mathbb{N}_\omega(i,j,k)$ for each voxel (i,j,k); ϵ, the predefined threshold of the stop condition of CMEWCVT; and S, a set of constraint slices with human annotated segmentation.

In the experiments, we chose $L = 5$, $\lambda = 500$. Considering the size of carbides and the energy balance, (see discussions in [17]), we set $\omega = 6$, and $\mathbb{N}_\omega(i,j,k)$ to be a sphere centered at voxel (i,j,k). Theoretically, Algorithm 3-CMEWCVT stops when the energy function Eqn. (13) is completely minimized. However, in practical applications, we can set the stop condition as

$$\frac{|E_{i+1} - E_i|}{E_i} < \epsilon \tag{16}$$

where E_i denotes the CMEWVT energy at the i-th iteration and ϵ is a predefined threshold. In the experiments, we selected $\epsilon = 10^{-4}$. In addition, we chose different number of constraint slices and analyze the affect to the segmentation accuracy. In our experiments, we tried $3, 6, 9, 12, 15, 18$ and 21 constraint slices.

To quantitatively evaluate the accuracy and performance of the CMEWCVT algorithm, we calculated its boundary accuracy against the manually annotated ground-truth segmentation and compared the boundary accuracy with other segmentation/boundary-detection methods. Besides the MCEWCVT [1], we also compare the segmentation accuracy with meanshift [4], SRM [6], pbCanny edge detector [20], pbCGTG edge detector [20], gPb [21] and watershed [5].

For the MCEWCVT algorithm [1] and the proposed CMEWCVT algorithm, we examine the segmentation boundaries on the 170 non-interpolated image slices. For other 2D comparison methods, we tested them directly on 170 non-interpolated slices. For the segmentation methods that are developed only for single-channel images, we applied them on each of the four channels independently and then combine the segmentation results from all four channels to get a unified segmentation for each slice. Specifically, for Pb edge detectors, at each pixel we took the maximum Pb value over all four channels. For the other comparison methods, we combined the segmentations from all four channels using a logic OR operation.

For the quantitative comparison, we used segmentation evaluation codes provided in the Berkeley segmentation benchmark [20] to calculate the precision-recall

and F-measure(harmonic mean of the precision and recall), which is in the form of

$$F = 2 \cdot \frac{precision \cdot recall}{precision + recall}.$$

For the CMEWCVT algorithm, we evaluated the average best F-measure for Case I: over all non-interpolated slices but the constraint slices; and Case II: over all non-interpolated slices including the constraint slices. For the other comparison algorithms, include MCEWCVT and the 2D image segmentation algorithms, we evaluated the average best F-measure over all the 170 superalloy image slices.

For the Pb based edge detectors, varying the threshold on a soft boundary map can produce a series of binarized boundary images, with which a precision-recall curve can be calculated and a best F-measure can be obtained to measure the segmentation performance. For the other comparison methods, binary segmentation boundaries leads to a single precision-recall value, from which we can compute a F-measure. Generally, the higher the F-measure, the better the segmentation. From Table 1, it is easy to see that the proposed CMEWCVT algorithm achieves the best F-measures of 93.6% and 94.3% in Case I and Case II, respectively, which significantly outperforms the MCEWCVT (F-measure: 89%) and other six 2D segmentation/edge-detection methods. Here, we set $\omega = 6$, and $\lambda = 500$, and use 21 constraint slices.

Table 1. Segmentation performance of the proposed CMEWCVT algorithm and its comparison methods. The F-measure of CMEWCVT is based on using 21 constraint slices.

Methods	CMEWCVT (Case I)	CMEWCVT (Case II)	MCEWCVT	gPb	pbCanny
F-measure	93.6%	94.3%	89%	85%	83%
Methods	pbCGTG	meanshift	SRM	watershed	
F-measure	82%	81%	80%	31%	

Figure 3 shows a visual comparison between the segmentation results of CMEWCVT and MCEWCVT on a few selected image slices. We can see that, different intensity variation is allowed within each grain by following human annotated segmentation. This way, compared with MCEWCVT, many small over-segmentation errors are suppressed in the proposed CMEWCVT. Meanwhile, the intensity difference between neighboring grains are better defined by human annotated segmentation. As a result, some under-segmentation errors in MCEWCVT are corrected in CMEWCVT.

We also conducted experiments to analyze the affect of using different number of constraint slices. As mentioned above, we tried the use of 3, 6, 9, 12, 15, 18 and 21 constraint slices which are all uniformly distributed across the whole 3D superalloy image volume and Table 2 shows the resulting F-measures for Case I. As we can see, the F-measure increases as we use more constraint slices. This validates the proposed idea that incorporating prior knowledge from material

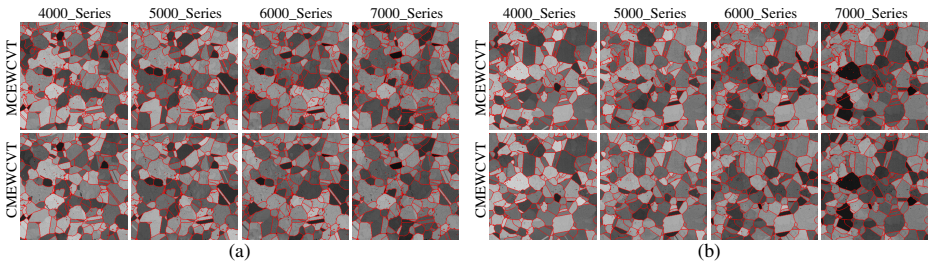

Fig. 3. Visual comparisons (two slices, (a) and (b) between the segmentation results of the proposed CMEWCVT algorithm and the MCEWCVT algorithm

scientists can substantially improve the segmentation performance. In addition, the more the constrained slices, the better the performance. Table 3 shows the segmentation performance for Case II.

Table 2. The comparison of the segmentation accuracy when using different number of constraint image slices. The numbers in this table are calculated without taking constraint image slices into account (Case I).

Number of constraint slices	3	6	9	12	15	18	21
Average Recall	90.7%	93%	93%	89.5%	90.3%	90.8%	94.3%
Average Precision	90.9%	89.5%	89.8%	94.5%	94.9%	94.7%	92.9%
F-measure	90.8%	91.2%	91.3%	91.9%	92.5%	92.7%	93.6%

Table 3. The comparison of the segmentation accuracy when using different number of constraint image slices when taking constraint image slices into account (Case II)

Number of constraint slices	3	6	9	12	15	18	21
Average Recall	90.8%	93.2%	93.3%	90.2%	91%	91.6%	94.9%
Average Precision	91%	89.9%	90.3%	94.9%	95.4%	95.2%	93.7%
F-measure	90.9%	91.5%	91.8%	92.5%	93.1%	93.4%	94.3%

From Fig. 4, another observation from the experiments is that the improvement of the average F-measure from CMEWCVT is contributed by almost all the superalloy image slices. In another word, by introducing the constraint slices, the segmentation on almost all the other slices are improved, instead of just the few slices near to the constraint slices. This indicates the prior knowledge provided by the constraint slices can be propagated to the whole 3D volume image by using the proposed CMEWCVT. In addition, almost all the slices have the F-measure around 0.9 or even higher except for the 40-th slice which has the F-measure around 0.7 due to its poor imaging quality.

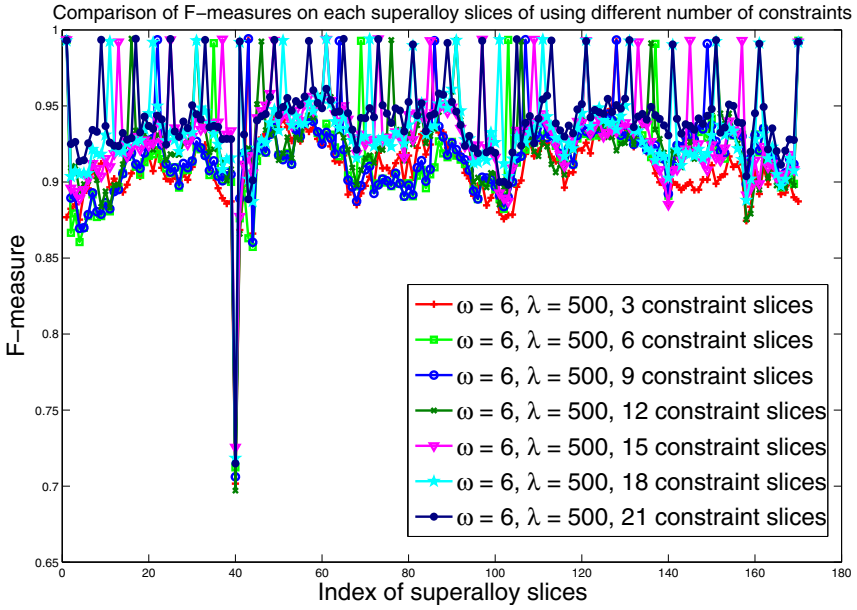

Fig. 4. F-measure computed from each superalloy image slice when using different number of constraint slices

6 Conclusions

In this paper, we developed a constrained multichannel edge-weighted centroidal Voronoi tessellations (CMEWCVT) algorithm for the purpose of 3D superalloy grain image segmentation. Compared to the previous MCEWCVT algorithm, the proposed algorithm can incorporate the human annotated segmentation on a small set of superalloy slices as constraints for the MCEWCVT energy minimization. As a result, the professional prior knowledge from material scientists can indeed be incorporated to produce much better segmentation results as demonstrated by our experiments.

Acknowledgments. This work was supported, in part, by AFOSR FA9550-11-1-0327, NSF IIS-0951754, NSF IIS-1017199, NSF DMS-0913491, NSF DMS-1215659 and ARL under Cooperative Agreement Number W911NF-10-2-0060 (DARPA Mind's Eye). The views and conclusions contained in this document are those of the authors and should not be interpreted as representing the official policies, either express or implied, of AFOSR, NSF, ARL or the U.S. Government. The U.S. Government is authorized to reproduce and distribute reprints for Government purposes, notwithstanding any copyright notation herein.

References

1. Cao, Y., Ju, L., Zou, Q., Qu, C., Wang, S.: A multichannel edge-weighted centroid Voronoi tessellation algorithm for 3D superalloy image segmentation. In: CVPR, pp. 17–24 (2011)
2. Reed, R.C.: The Superalloys Fundamentals and Applications. Cambridge Press (2001)
3. Voort, G.F.V., Warmuth, F.J., Purdy, S.M.: Metallography: Past, Present, and Future (75th Anniversary Vol.). Astm Special Technical Publication (1993)
4. Comaniciu, D., Meer, P.: Mean shift: A robust approach toward feature space analysis. TPAMI 24, 603–619 (2002)
5. Meyer, F.: Topographic distance and watershed lines. Signal Processing 38, 113–125 (1994)
6. Nock, R., Nielsen, F.: Statistical region merging. TPAMI 26, 1425–1458 (2004)
7. Shi, J., Malik, J.: Normalized cuts and image segmentation. TPAMI 22, 888–905 (1997)
8. Felzenszwalb, P.F.: Efficient graph-based image segmentation. IJCV 59, 167–181 (2004)
9. Li, C., Xu, C., Gui, C., Fox, M.D.: Level set evolution without re-initialization: A new variational formulation. In: CVPR, pp. 430–436 (2005)
10. Couprie, C., Najman, L., Grady, L., Talbot, H.: Power watersheds: A new image segmentation framework extending graph cuts, random walker and optimal spanning forest. In: ICCV, pp. 731–738 (2009)
11. Cousty, J., Bertrand, G., Najman, L., Couprie, M.: Watershed cuts: thinnings, shortest-path forests and topological watersheds. TPAMI 32, 925–939 (2010)
12. Chuang, H.-C., Huffman, L.M., Comer, M.L., Simmons, J.P., Pollak, I.: An automated segmentation for Nickel-based superalloy. In: ICPR, pp. 2280–2283 (2008)
13. Boykov, Y., Funka-Lea, G.: Graph cuts and efficient N-D image segmentation. IJCV 70, 109–131 (2006)
14. Grady, L.: Random walks for image segmentation. TPAMI 28, 1768–1783 (2006)
15. Whitaker, R.T.: A level-set approach to 3D reconstruction from range data. IJCV 29, 203–231 (1998)
16. Magee, D., Bulpitt, A., Berry, E.: Level set methods for the 3D segmentation of CT images of abdominal aortic aneurysms. In: Medical Image Understanding and Analysis, pp. 141–144 (2001)
17. Wang, J., Ju, L., Wang, X.: An edge-weighted centroidal Voronoi tessellation model for image segmentation. IEEE TIP 18, 1844–1858 (2009)
18. Powell, M.J.D.: An efficient method for finding the minimum of a function of several variables without calculating derivatives. Computer Journal 7, 152–162 (1964)
19. Du, Q., Faber, V., Gunzburger, M.: Centroidal Voronoi tessellations: applications and algorithms. SIAM Review 41, 637–676 (1999)
20. Martin, D.R., Fowlkes, C., Tal, D., Malik, J.: A database of human segmented natural images and its application to evaluating segmentation algorithms and measuring ecological statistics. In: ICCV, pp. 416–423 (2001)
21. Arbelaez, P., Maire, M., Fowlkes, C., Malik, J.: Contour detection and hierarchical image segmentation. TPAMI 33, 898–916 (2011)